NCA-Vol. 27, Proceedings of the ASME
Noise Control and Acoustics Division — 2000
ASME 2000

SILICON MICROMACHINED ULTRASONIC TRANSDUCERS

Butrus T. Khuri-Yakub, Ching-Hsiang Cheng,
Fahrettin-Levent Degertekin, Sanli Ergun,
Sean Hansen, Xue-Cheng Jin, and Omer Oralkan

Edward L. Ginzton Laboratory
Stanford University
Stanford, CA 94305-4085
USA

ABSTRACT

This paper reviews capacitor micromachined ultrasonic transducers (cMUTs). Transducers for air-borne and immersion applications are made from parallel-plate capacitors whose dimensions are controlled through traditional integrated circuit manufacturing methods. Transducers for airborne ultrasound applications have been operated in the frequency range of 0.1-11 MHz, while immersion transducers have been operated in the frequency range of 1-20 MHz. The Mason model is used to represent the cMUT and highlight the important parameters in the design of both airborne and immersion transducers. Theory is used to compare the dynamic range and the bandwidth of the cMUTs to piezoelectric transducers. It is seen that cMUTs perform at least as well if not better than piezoelectric transducers. Examples of single-element transducers, linear-array transducers, and two-dimensional arrays of transducers will be presented.

1. INTRODUCTION

Capacitors have long been used as ultrasound transducers [1]. Conventional designs have relatively large gaps, 50-100 μm, and use the air in the gap as the restoring force of the vibrating electrode. These transducers thus suffer from low efficiency because of the relatively large gap height. We propose a design where silicon micromachining is used to define the capacitors. The gaps are made to be as small as 500 Å, and the restoring force of the vibrating electrode is the stiffness of the electrode itself. This approach makes possible the fabrication of very efficient transducers, indeed, it makes possible transducers that compete with piezoelectric transducers in terms of efficiency and bandwidth [2,3]. One advantage of these transducers that they allow integration of electronics components on the same silicon wafer. Another is the potential for fabricating one-dimensional, two-dimensional, and annular arrays of transducers using simple photolithography.

2. ELECTRICAL EQUIVALENT CIRCUIT MODEL OF THE TRANSDUCER

We use Mason's model to represent the capacitor transducer [4]. A schematic of the transducer and its equivalent circuit are shown in Fig. 1. A metal-coated silicon nitride membrane is used as the vibrating electrode of the capacitor. Standard integrated manufacturing processes are used to define the dimensions of the capacitor. Residual stress in the membrane is controlled via the process of chemical vapor deposition and is held at around 100 MPas [5].

In the equivalent circuit, C_0 is the capacitance of the device, Z_s is the impedance of the source, Z_a is the impedance of the medium (air or water), and Z_m is the mechanical impedance of the circular membrane of radius 'a" which is given by:

$$Z_m = j\omega\rho l_t \frac{ak_1k_2\left(k_2J_0(k_1a)J_1(k_2a)+k_1J_1(k_1a)J_0(k_2a)\right)}{ak_1k_2\left(k_2J_0(k_1a)J_1(k_2a)+k_1J_1(k_1a)J_0(k_2a)\right)-2\left(k_1^2+k_2^2\right)J_1(k_1a)J_1(k_2a)} \quad (1)$$

where ω is the radian frequency, ρ is the density of the membrane, l_t is the thickness of the membrane, J_0 and J_1 are the zeroth and first-order Bessel functions of the first kind and k_1 and k_2 are given by:

$$k_1 = \sqrt{\frac{\sqrt{d^2+4c\omega^2}-d}{2c}},\ k_2 = \sqrt{\frac{\sqrt{d^2+4c\omega^2}+d}{2c}},\ c = \frac{(Y_0+T)l_t^2}{12\left(1-\sigma^2\right)} \text{ and } d = \frac{T}{\rho}, \quad (2)$$

where Y_0 is Young's modulus, T is the residual stress and σ is the Poisson's ratio of the membrane material. The impedance of the membrane can be represented by a

series resistance-inductance-capacitance (RLC) circuit with a resistance corresponding to the loss in the membrane.

The transformer ratio in the equivalent circuit is given by:

$$n = V_{dc} \frac{\varepsilon_0 \varepsilon^2 S}{(\varepsilon_0 l_t + \varepsilon l_a)^2}, \tag{3}$$

where V_{dc} is the dc bias on the electrode, ε_0 is the dielectric constant of the free space, ε is the dielectric constant of the membrane material, S is the area of the transducer and l_a is the thickness of the air gap.

The importance of the approach we propose lies in the fact that the transformer ratio can be made very large. The capacitance of the capacitor can be 10 s of pFs, and the electric field can be as high as 10^9 V/m. This high electric field is achieved because the gap of the capacitor can be made to be as small as 500 Å. It is easy to see why the sensitivity of these capacitors is markedly higher than that of the earlier designs. The gap being several orders of magnitude smaller results in a relative change in capacitance that is the same number of orders of magnitude higher.

In a typical capacitor, each membrane is in the range of 20-100 microns in diameter. Thus, to fabricate a transducer, a very large number of membranes are electrically connected in parallel using a lithography step. This use of lithography allows the manufacture of single elements, or array elements side by side on the same wafer and in one step.

In an air transducer, the impedance of the membrane at resonance is zero and comparable in value to the impedance of air over the bandwidth. The transducer exhibits a characteristic RLC resonant behavior. Without dc bias, the real part of the input impedance is zero and the imaginary part is that of a capacitor. As dc bias is applied, the resonant membrane introduces a real resistance resonant peak that represents real power coupled into the sound, and the imaginary part shows the characteristic acoustic "N" corresponding to potential and kinetic energy storage.

In immersion transducers, the impedance of the membrane is smaller than the impedance of water and can be ignored. Thus, the input impedance of an immersion transducer has no resonance and consists only of an RC circuit in series (or parallel) [6]. Thus, impedance matching of the electronics to the RC circuit determines the bandwidth and efficiency of the transducer.

The performance of a cMUT and a piezoelectric transducer are compared. For comparison, we use a square element with a side of 0.4 mm as the subject of our research program. The design calls for a center frequency of operation of 3 MHz with a bandwidth enabling operation at 0.75 MHz. The KLM model is used to represent the piezoelectric transducer, and the Mason model outlined above is used to represent the cMUT. For the piezoelectric transducer, we use PZT 5H for the piezoelectric material and assume a perfect match into water using one matching layer. The cMUT has an air gap of 1500 Å, a silicon nitride membrane thickness of 8000 Å, a cell radius of 18 μm, and operates at a dc voltage of 100 V.

The performance of each device as a transmitter is determined by calculating the pressure at the face of the transducer that is generated by applying 1 V at its input terminals. The receiver sensitivity is calculated by evaluating the signal to noise level of the received voltage for an input pressure of 1 Pa at the face of the transducer. This signal to noise is calculated assuming an amplifier with an input resistance of 300 kΩ and capacitance of 0.3 pF. The total dynamic range of the system is calculated by adding together the transmitter and the receiver sensitivities for each transducer. Fig. 2 shows the results of this comparison.

It is seen from Fig. 2 that the cMUT can have as good a dynamic range as a piezoelectric transducer over a much larger bandwidth. The minimum insertion loss and bandwidth are determined by electrical matching considerations of the transducer to the electronic circuit.

3. TRANSDUCER FABRICATION

Standard integrated circuit fabrication processes are used to fabricate the cMUT. Figure 3 shows the process presently used for fabricating transducers. First, the silicon wafer receives a high-doping-density ion implantation for formation of the back contact of the capacitor. Then, a layer of insulating silicon nitride is deposited to protect the back contact and as an etch stop. An amorphous silicon sacrificial layer is deposited over the wafer. The sacrificial layer is defined by photolithography. The amorphous silicon is left in regions that are to become vacuum gaps. Another silicon nitride layer is deposited over the amorphous silicon. Holes are defined at the edges of the amorphous silicon which are then removed by wet etching. Silicon nitride is again deposited and used to plug the holes through which the etching fluid was introduced. Finally, an aluminum layer is deposited over the wafer to define the top electrode of the capacitor. An optical image of a finished device is shown in Fig. 4.

The individual cells are connected electrically in parallel using aluminum metal. The metal over each cell is clearly seen to be one half of the diameter of each cell. The size of the electrode is decreased to reduce the capacitance of the device without reducing the displacement at the surface of the membrane.

4. EXPERIMENTAL RESULTS

Immersion and air transducers are evaluated via measurements of their electrical input impedance, input response and bandwidth, beam profile and insertion loss. In order to fit the measured impedance of a transducer to the theoretically predicted value, a loss term has to be added to account for the insertion loss of the transducer, and a parasitic capacitance term has to be included to accurately predict the imaginary part of the impedance.

The impulse response of an immersion transducer is shown in Fig. 5. The impulse response of the transducer shows the large bandwidth that is characteristic of cMUTs. The measured fractional bandwidth is over 100%, which is limited by the electronics and not the transducer. Measurement of the insertion loss of the device shows that there is a one-way loss of 5 dB that is due to coupling into the propagation modes of the wafer.

Air transducers perform in a manner similar to immersion transducers. The main difference is that the fractional bandwidth is of the order of 5%. This small bandwidth is a result of the device performance being dominated by the resonance of the membrane. Fig. 6 shows the impulse response of an air transmission experiment. Two identical transducers are used to transmit and receive a 2.3 MHz 20-cycle tone burst after propagation through an aluminum sample. The distance between the transducers and the sample is 3mm, while the thickness of the sample is 6.25 mm. Transmission through aluminum indicates that the transmission system has a dynamic range of over 100 dB. The air transducers have a one way insertion loss of 10 dB. This loss is due to the coupling of a Lamb wave into the structure [8].

One of the main features of the cMUT technology is that it allows the use of photolithography to define 1-D or 2-D arrays. Another feature of cMUT arrays is that they have a thin profile, equal to the thickness of the silicon wafer. Thus, arrays can be made small to fit in tight spaces. Electronic circuits can be integrated on the same wafer as the transducers. Or, the transducer wafer can be flip-chip bonded to an electronics wafer without a significant increase in the profile of the array.

Figure 7 shows a 64-element 1-D array. The elements of the 1-D array are on 0.4 mm centers and are each 5.6 mm long. Each element consists of a number of

cells that are connected in parallel in the same fashion as in single-element transducers.

The 64-element 1-D array was used to image a 0.4 mm x 0.4 mm (active area of 0.28 mm x 0.28 mm) transmitter which is placed 5 cm away in the plane perpendicular to the center of the array. The point source is excited with a pulse and all 64 elements in the array are used to receive the signal from the transmitter. Each received signal has a time delay associated with the distance between the transmitter and receiver. Simple time-delay reconstruction of the raw rf data was carried out to image the field of view in front of the array. The result of this electronic reconstruction is shown in Fig. 8.

The elements of the 1-D array excite Lamb waves in the silicon wafer. This energy leaks back into the fluid and introduces ripples in the beam profile of an array element. A typical beam profile of a single element, in the plane perpendicular to the array element's surface, is shown in Fig. 9. This problem with the beam profile of an array element can be reduced by thinning the wafer, as seen in Fig. 9, or by adding porous silicon or trenches between array elements.

Two-dimensional arrays can also be made using the same process as described above. However, there needs to be some means to connect each individual element. One method for establishing electrical connection to each element in the 2-D array is through-wafer holes as shown in Fig. 10. Again, each element of the 2-D array is constructed by connecting in parallel a number of individual cells.

The beam profile of a 2-D array element is measured in the same way as the 1-D array element. One difference is that the beam profile of a 2-D element is symmetric around the perpendicular to the face of the element. The measured acceptance angle is in excellent agreement with theoretical predictions, as shown in Fig. 11. There is a slight ripple in the acceptance angle at 12° and 22° where the lowest-order antisymmetric and symmetric Lamb waves are excited at 4 MHz in a 0.5-mm-thick silicon wafer. This problem is small and can be further reduced as mentioned earlier.

The dynamic range of a 2-D element in the array is measured using a calibrated hydrophone (Specialty Engineering Associates model # PZT-Z44-0400). The output pressure at the face of the transducer, for an input voltage of 1 V, is about 20 kPa with a flat frequency response from 1 MHz to 10 MHz over the range of calibration of the hydrophone. The receiver signal-to-noise ratio is 45 dB/Pa/Hz. As seen from Fig. 12, the total dynamic range is then found to be about 130 dB/Volt/Hz. This dynamic range can be further increased by 10 dB using an amplifier with a better

noise figure and by reducing the parasitic capacitance of the device. The minimum detectable pressure was measured to be 5 mPa/$\sqrt{Hz}$, which corresponds to a detectable displacement of $2.5x10^{-16}$ m/$\sqrt{Hz}$. Again, this minimum detectable noise floor can be further reduced by using a lower noise amplifier and a transducer element with a lower parasitic capacitance. The dynamic range plot shows a ripple around 1.5 MHz, which is further evidence of the coupling into Lamb waves that can be reduced.

5. CONCLUSIONS

Silicon micromachining can be used to fabricate capacitive ultrasonic transducers that can compete with piezoelectric transducers in terms of efficiency and bandwidth. The main reason for the promise of cMUTs is the fact that the electric field in the gap of the capacitors can be made as high as 10^9 V/m. Researchers in the field have recognized this fact for almost 100 years now, only the advent of silicon micromachining has enabled this capability and brought cMUTs to the competitive edge they now demonstrate. Theory predicts the performance, and only manufacturing and characterization issues remain to be solved. Besides performance, silicon micromachining also adds the promise of ease of manufacture of 1-D and 2-D arrays and of integration with electronic circuitry.

ACKNOWLEDGMENTS

We are grateful for the support of the Defense Advanced Research Agency, the Air Force Office of Scientific Research, and the Office of Naval Research.

REFERENCES

1. W. Khul, G.R. Schodder, and F.K. Schodder," Acustic*a*, Vol. 4, p. 520 (1954).
2. M.I. Haller and B.T. Khuri-Yakub, IEEE Trans. UFFC, Vol. 43, p. 1 (1996).
3. I. Ladabaum, T. Soh, X.C. Jin, A. Atalar and B.T. Khuri-Yakub, IEEE Trans. UFFC, Vol. 45, p. 698 (1998).
4. W. P. Mason: *Electromechanical Transducers and Wave Filters*, 2nd ed (1948).
5. X.C. Jin, I. Ladabaum, and B.T. Khuri-Yakub, IEEE/ASME J. Micro-Electro-Mechanical Syst., Vol. 7, p. 295 (1998).
6. X.C. Jin, I. Ladabaum, and B.T. Khuri-Yakub, Proceedings of the IEEE Workshop on Microelectromechanical Systems (1998), p. 649.
7. X.C. Jin, F.L. Degertekin, S. Calmes, X.J. Zhang, I. Ladabaum, and B.T. Khuri-Yakub, Proceedings of the IEEE Ultrasonic Symposium, 1877 (1998), p. 1877.
8. A. Bozkurt, F.L. Degertekin, A. Atalar, and B.T. Khuri-Yakub, Proceedings of the IEEE Ultrasonic Symposium (1998), p. 1025.

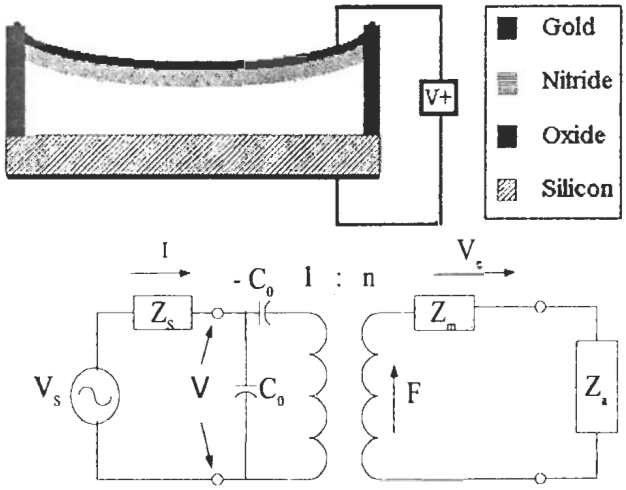

Fig. 1 Schematic diagram of a capacitor transducer and its electrical equivalent circuit.

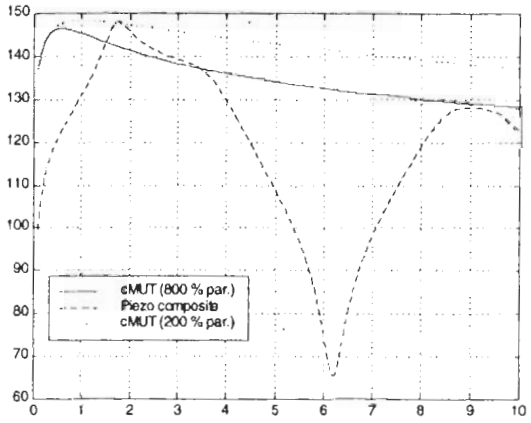

Fig. 2 Comparison of the dynamic ranges of a cMUT and a piezoelectric transducer.

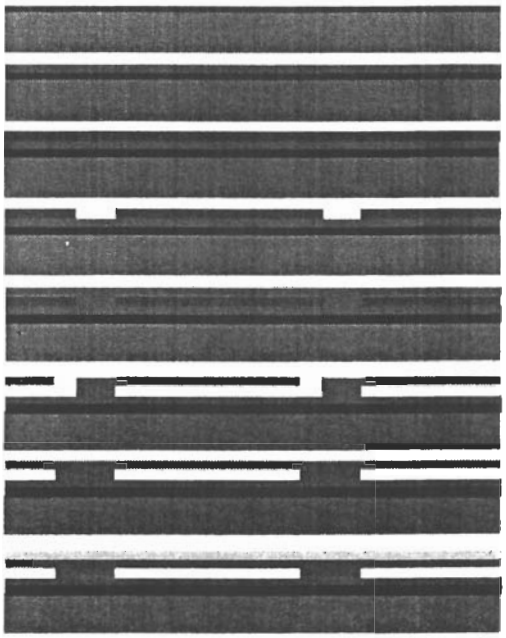

Fig. 3 Schematic of the processing schedule for fabricating cMUTs.

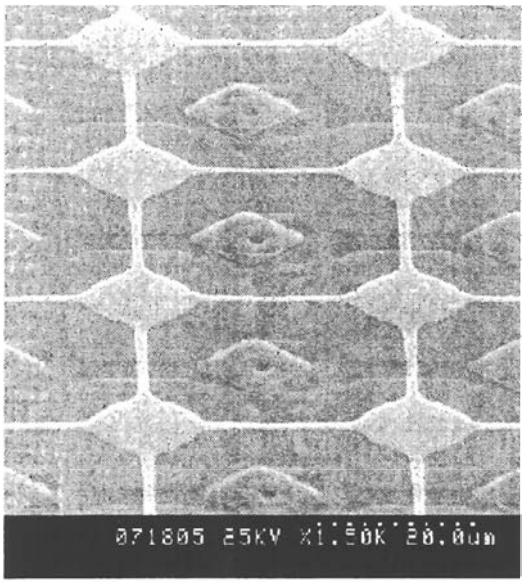

Fig. 4 A finished cMUT.

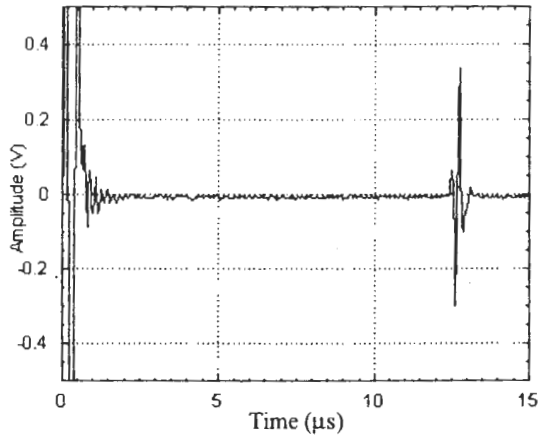

Fig. 5 Impulse response of an immersion cMUT transducer.

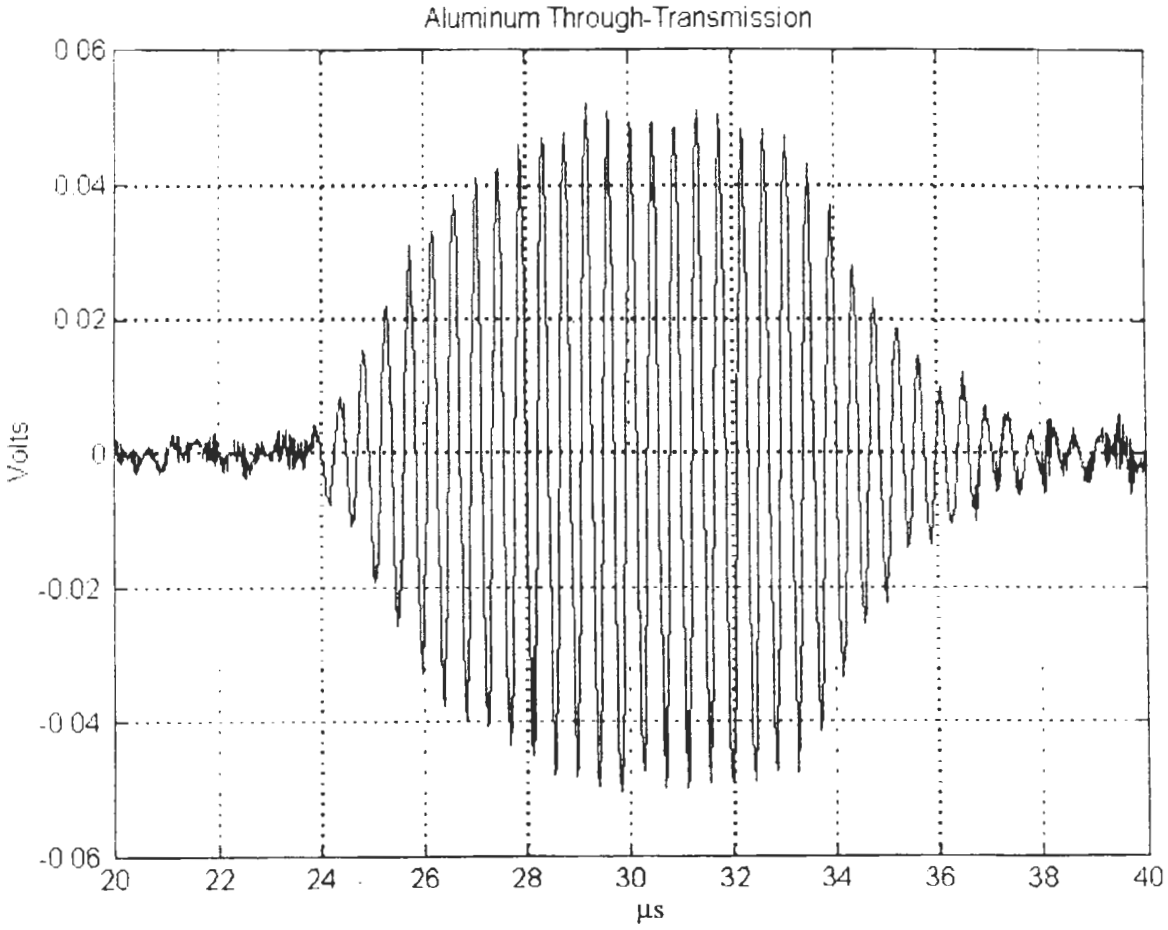

Fig. 6 Airborne ultrasound pulse transmission through an aluminum sample.

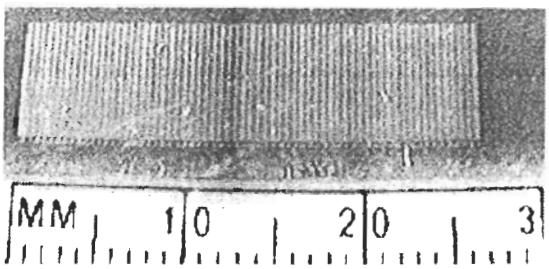

Fig. 7 A 1-D array of transducers.

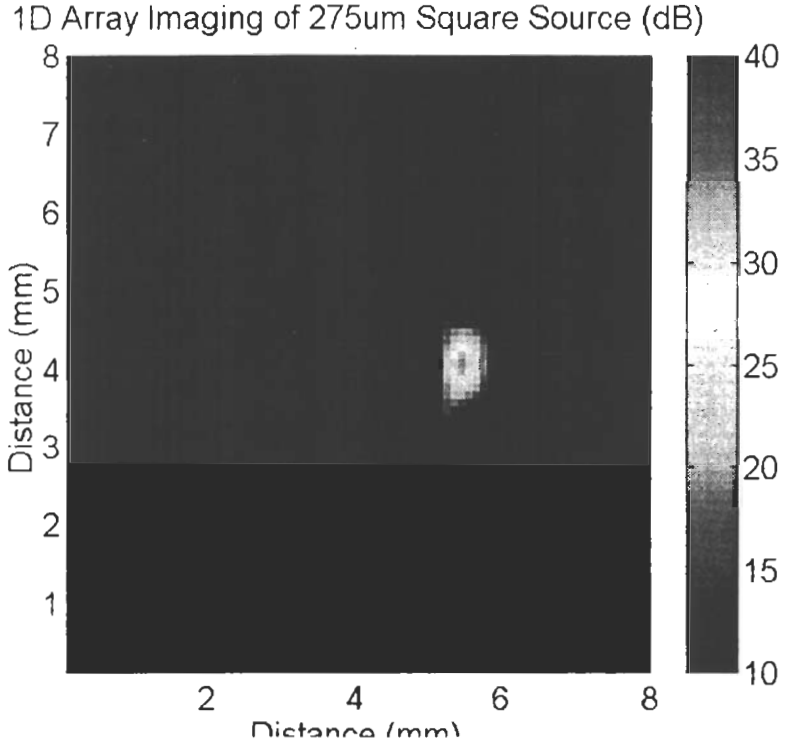

Fig. 8 Reconstructed image of a 0.4 mm x 0.4 mm point source.

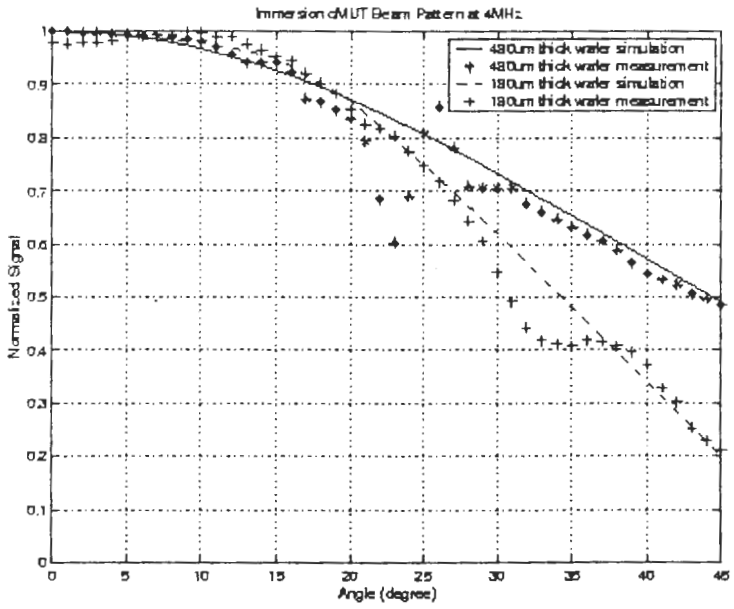

Fig. 9 Measured versus calculated acceptance angle of an element of a 1-D array at a frequency of 4 MHz.

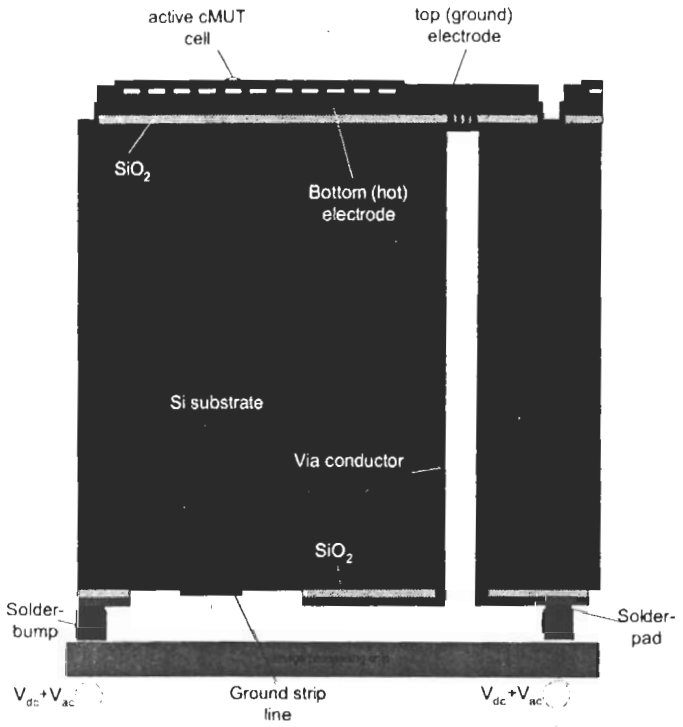

Cross section through one array element

Fig. 10 Schematic diagram of a 2-D array element with a through-wafer hole.

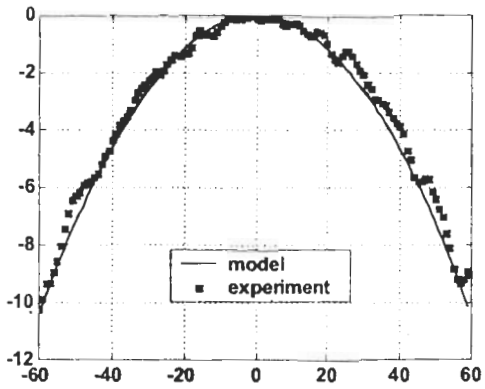

Fig. 11 Beam profile of a 0.4 mm x 0.4 mm element of a 2-D array at a frequency of 3 MHz.

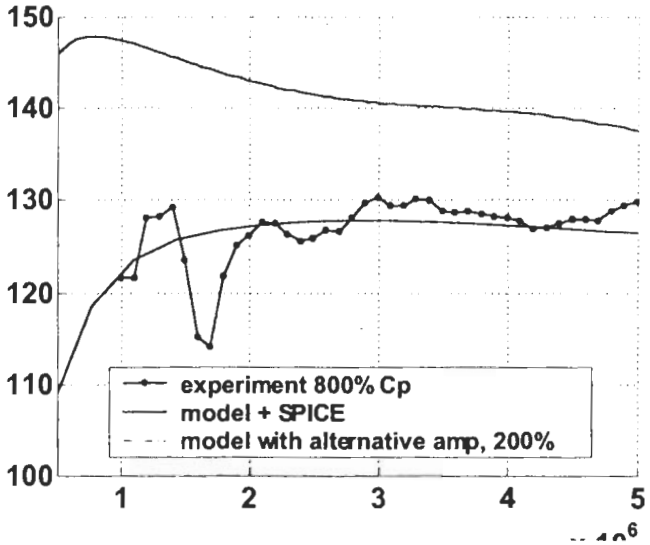

Fig. 12 Measured dynamic range of a 0.4 mm x 0.4 mm element of a 2-D array element.